# Applications of optimal time-domain beamforming

Michael D. Collins, Jonathan M. Berkson, W. A. Kuperman, Nicholas C. Makris, and John S. Perkins
*Naval Research Laboratory, Washington, DC 20375*

(Received 24 July 1992; accepted for publication 17 December 1992)

Applications to ocean acoustic data from a towed array and to speech processing are presented for an improved optimal time-domain beamformer, which involves optimizing over all possible source bearings and time series for multiple sources using simulated annealing. The convergence of the parameter search is accelerated by accepting time series perturbations only when the energy decreases. A comparison with the conventional delay-and-sum beamformer illustrates that the optimal beamformer handles larger receiver spacing and larger source-to-receiver ratio. Periodic ambiguities are essentially eliminated by using irregular receiver spacing and the improved search algorithm. Weak sources are handled with fractional beamforming. Noise cancellation is possible if the parameters of the noise are included in the search space. Two-dimensional localization is performed for nearby sources.

PACS numbers: 43.30.Yj, 43.60.Gk

## INTRODUCTION

Conventional beamforming techniques, such as the delay-and-sum beamformer, involve an ambiguity function that depends on a single parameter corresponding to source bearing. The estimates of the source bearings correspond to the peaks in the ambiguity function. Considering that conventional beamforming techniques involve collapsing a large number of parameters (the source bearings and time series) into a single parameter (the steering parameter of the ambiguity function), it is rather amazing that they often perform well for problems involving multiple sources.

The optimal beamformer estimates the source bearings and time series all at once by optimizing an energy function that depends on all of the source bearings and time series.[1] This beamformer, which is a generalization of a frequency-domain beamformer,[2] is practical with simulated annealing, an efficient Monte Carlo method for optimization problems involving large numbers of parameters.[3,4] By working with all of the unknowns, the optimal beamformer easily utilizes and benefits from *a priori* information.[1] The only approach for utilizing *a priori* information with conventional beamforming is to define a new ambiguity function, which by conservation is likely to inhibit performance in some way. In this paper, we improve the search algorithm for the optimal beamformer, demonstrate that the optimal beamformer permits a larger source-to-receiver ratio than the delay-and-sum beamformer, and apply the optimal beamformer to data.

To implement the optimal beamformer numerically, the source time series are discretized. This often amounts to thousands of unknown parameters. Since the energy function passes through a unique minimum as one of the discretized time series points is varied, an improved simulated annealing algorithm is obtained by accepting time series perturbations only if the energy is decreased. Since the energy function may pass through local minima as one of the bearings is varied, the usual acceptance criterion of simulated annealing is used for the bearings: A perturbation is always accepted if the energy decreases and, to allow escape from local minima, is accepted according to the Boltzmann probability distribution if the energy increases. An example is presented in Sec. II that illustrates the accelerated convergence of the improved algorithm.

In Sec. III, the optimal beamformer is compared with the delay-and-sum beamformer. Although it is not possible in general to place a limit on the number of sources that can be handled by a particular array (e.g., bearings may be determined for an unlimited number of cw sources of different frequencies), the delay-and-sum beamformer typically requires several times the number of receivers that the optimal beamformer requires. An example is presented to illustrate that, for a given array of receivers, the optimal beamformer may perform well, while the delay-and-sum beamformer completely fails with large false peaks. In Sec. IV, we illustrate an advantage of using irregularly spaced receivers. Combined with the new search algorithm, irregular spacing essentially eliminates time series ambiguities associated with periodic functions.

A method that we refer to as fractional beamforming is described in Sec. V. With this approach, the optimal beamformer is first applied to estimate the bearings and time series of the most intense sources. These signals are subtracted from the data, and the reduced data are then searched for weaker sources. If the intense signals dominate the received time series, this approach can be more effective than searching for all of the sources at once. In Sec. VI, we generalize the search algorithm to cancel noise, which is possible if something is known about the nature of

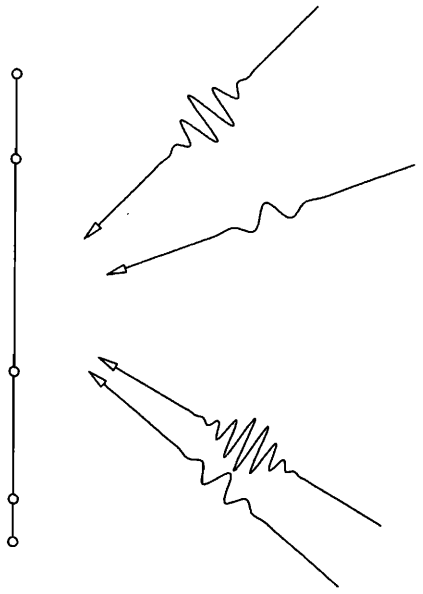

FIG. 1. An example configuration of the array and sources: Four plane-wave time series arriving at a linear array of five hydrophones from different bearings.

the noise. In Sec. VII, we generalize the optimal beamformer to the case of incident spherical waves for two-dimensional localization.

The performance of the optimal beamformer is robust for data. A speech processing application of optimal beamforming is presented in Sec. VIII. This problem involves a very large number of parameters and complex signals. The voices of speakers in a noisy crowd are isolated, and the recovered voices sound free of interference from the other voices. In Sec. IX, the optimal beamformer is applied to data from an array towed in the Atlantic Ocean. The approach of Sec. VI is used to cancel noise from this data. The optimal beamformer replicas are surgically removed from the data, and a conventional beamformer is used to process the reduced data.

## I. THE OPTIMAL BEAMFORMER

As illustrated in Fig. 1, a linear array of sensors receives the $M$ plane-wave acoustic signals $p_m(t)$ from the directions $\theta_m$. A subset of the source bearings and each of the signal time series are unknown. The signal $P_n(t)$ received by the $n$th receiver is

$$P_n(t)=\sum_{m=1}^{M} p_m(t+\tau_n \sin\theta_m)+\Psi_n(t). \tag{1}$$

The delays $\tau_n=x_n/c$ are defined in terms of the hydrophone locations $x_n$ and the sound speed $c$. The noise term $\Psi_n(t)$ may be due to additional sources, ambient noise, and other types of noise. The replica signal $Q_n(t)$ received by the $n$th receiver is defined by

$$Q_n(t)=\sum_{m=1}^{M} q_m(t+\tau_n \sin\phi_m), \tag{2}$$

where the test parameters $q_m(t)$ and $\phi_m$ are the test time series and test bearings. The optimal beamformer estimate for $p_m(t)$ and $\theta_m$ is obtained by minimizing the energy,

$$E(q_1,\phi_1,\ldots,q_M,\phi_M)=\sum_{n=1}^{N}\int [P_n(t)-Q_n(t)]^2\,dt, \tag{3}$$

over the test parameters.

Each of the source time series is discretized so that the integral in Eq. (3) is approximated by a sum. Hundreds or thousands of points are typically used to represent each time series. The simulated annealing algorithm involves perturbing each parameter one at a time and evaluating $\Delta E$, the change in $E$. When one of the time series points is perturbed, only a few terms in the discretized integral are affected. Since $\Delta E$ can be computed efficiently, optimal beamforming is an excellent application of simulated annealing. Although all of the terms in the sum are affected when a source bearing is perturbed, this does not compromise efficiency because the number of source bearings is much smaller than the number of time series points.

The solution that minimizes $E$ may not be unique. For the case of evenly spaced receivers $x_n=n\,\Delta x$ and two sources, for example, $E$ vanishes for

$$q_1(t)=p_1(t)+f(t), \tag{4}$$

$$q_2(t)=p_2(t)-f(t), \tag{5}$$

where $f(t)$ is an arbitrary periodic function of period $(\Delta x/c)(\sin\theta_2-\sin\theta_1)$. This ambiguity, which involves multiple terms for problems involving more than two sources, was suppressed in Ref. 1 by assuming that the time series have compact support. This assumption is usually not valid for applications.

During the parameter search, the ambiguity does not present itself while the bearing parameters are wandering. After two or more of the bearings lock in, however, the ambiguous function(s) may grow without bound. In terms of the parameter landscape, this is analogous to entering a flat valley surrounded by mountains that get higher with distance into the valley. This is a serious problem because it is very difficult for simulated annealing to find a way out of this type of multidimensional valley. Fortunately, it is very unlikely to have a first encounter with such a valley at a point deep within because the signal time series tend to be uncorrelated when the bearings are wandering.

We illustrate in Sec. III that, in principle, all but the harmless dc component of the periodic ambiguity may be eliminated by using irregular receiver spacing. Since the time series are discretized, however, the high-frequency components are not entirely eliminated when using the simulated annealing algorithm of Ref. 1. When using the improved search algorithm described in Sec. II, the high-frequency components are also essentially eliminated.

## II. AN IMPROVED OPTIMIZATION ALGORITHM

Simulated annealing is an efficient method for solving optimization problems involving local minima and large numbers of unknowns. For specific applications, it is usually possible to tune this method to improve performance. For the beamforming problem, significant improvements were obtained by treating the bearings and time series as a mixture of two parameter types.[1] The energy change due to a perturbation of a point in the discretized time series is usually much smaller than the energy change due to a perturbation in the bearing of a source. If one were to treat all of the parameters the same, the bearings would freeze out of the mixture (usually at the wrong values) at a relatively high temperature. Using the analogy of the annealing of a crystal, this difficulty was overcome by scaling out the freezing-point difference in the acceptance probabilities.

In this section, we present an improved simulated annealing algorithm in which perturbations of the time series parameters are accepted only when the energy decreases. This approach is valid because the energy function is a parabola, which has a unique minimum, for each time series parameter. As with the simulated annealing algorithm of Ref. 1, each parameter is perturbed once during each iteration, one parameter at a time. As described in Ref. 1, the Boltzmann acceptance probability is used for the bearing perturbations, which are selected using a cubic distribution to allow the fast simulated annealing cooling schedule.[5] The time series perturbations are selected with the approach described in Ref. 1, but only those perturbations that lower the energy function are accepted.

The improved algorithm suppresses the high-frequency components of the periodic ambiguity, which is described in Sec. I for the two-source case. With the original algorithm, the ambiguous function does not begin to grow until after the bearings have locked in (not necessarily to the correct values) because the ambiguous signal components cancel each other only for a particular set of bearings. With the original algorithm, the ambiguous function may continue to grow after a nearly optimal state is reached, and the recovered signals usually contain higher frequencies than the data. With the improved algorithm, the ambiguous function does not grow after the bearings lock in and the energy function reaches a minimum, and the recovered signals tend to be as smooth as the data. In terms of the parameter landscape, the improved algorithm tends not to penetrate deeply into the flat valleys described in Sec. I because it only accepts downhill perturbations in the time series.

We illustrate the performance of the improved simulated annealing algorithm with example A, which was considered in Ref. 1 in terms of dimensionless variables. To repeat this example in dimensioned variables, we take $c=1000$ m/s and work in meters and milliseconds. Since the signals,

TABLE I. Data for the examples: $c$ is the speed of sound in m/s; $m$ is the source index; $\theta_m$ is the $m$th source bearing; $A_m$ is the $m$th source amplitude; and $\alpha_m$ is the time lag in ms for the $m$th Gaussian source, which is described by $\lambda_m$ and $w_m$ in ms.

| Example | $c$ | $m$ | $\theta_m$ | $A_m$ | $\alpha_m$ | $\lambda_m$ | $w_m$ |
|---|---|---|---|---|---|---|---|
| A,B,C | 1000 | 1 | 20° | 1 | −10 | 30 | 20 |
| | | 2 | −30° | −2 | 0 | 10 | 20 |
| | | 3 | 45° | 2 | 10 | 15 | 20 |
| | | 4 | −40° | 1 | 0 | 20 | 20 |
| | | 5 | −60° | −1 | −10 | 15 | 15 |
| D | 1000 | 1 | 20° | 1 | −10 | 30 | 20 |
| | | 2 | −30° | −10 | 0 | 10 | 20 |
| | | 3 | 45° | 10 | 10 | 15 | 20 |
| E | 1000 | 1 | 20° | 1 | −10 | 30 | 20 |
| | | 2 | −30° | −2 | 0 | 10 | 20 |
| | | 3 | 45° | 2 | 10 | 15 | 20 |
| F | 1000 | 1 | −30° | 3 | 0 | 10 | 20 |
| | | 2 | −30° | −1 | 0 | 15 | 30 |
| G | 300 | 1 | −40° | | | | |
| | | 2 | −20° | | | | |
| | | 3 | 15° | | | | |

$$p_m(t)=A_m \exp\left[-\left(\frac{t-\alpha_m}{w_m}\right)^2\right]\cos\left(\frac{2\pi(t-\alpha_m)}{\lambda_m}\right), \quad (6)$$

are of compact support, we assume compact support in the beamforming algorithm. The parameter values for the five sources are given in Table I. We take $\Delta x=20$ m for the seven equally spaced receivers. The received data appear in Fig. 2, and results appear in Figs. 3 and 4 for the original and improved algorithms. The improved algorithm converges to the correct source bearings several times faster than the original algorithm for this problem. The improved algorithm accurately recovers the source time series. Irregular receiver spacing is applied to this problem in Sec. IV.

## III. THE CONVENTIONAL BEAMFORMER

In this section, we compare the performance of the optimal beamformer and the delay-and-sum beamformer, which is defined by

$$B(\theta)=\int\left(\sum_{n=1}^{N} P_n(t-\tau_n \sin\theta)\right)^2 dt, \quad (7)$$

where $N \gg M$ and the steering parameter $\theta$ corresponds to source bearing. For the case $\Psi_n(t)\equiv 0$, we substitute Eq. (1) into Eq. (7) to obtain

$$B(\theta)=\int\left(\sum_{n=1}^{N}\sum_{m=1}^{M} p_m[t-\tau_n(\sin\theta-\sin\theta_m)]\right)^2 dt. \quad (8)$$

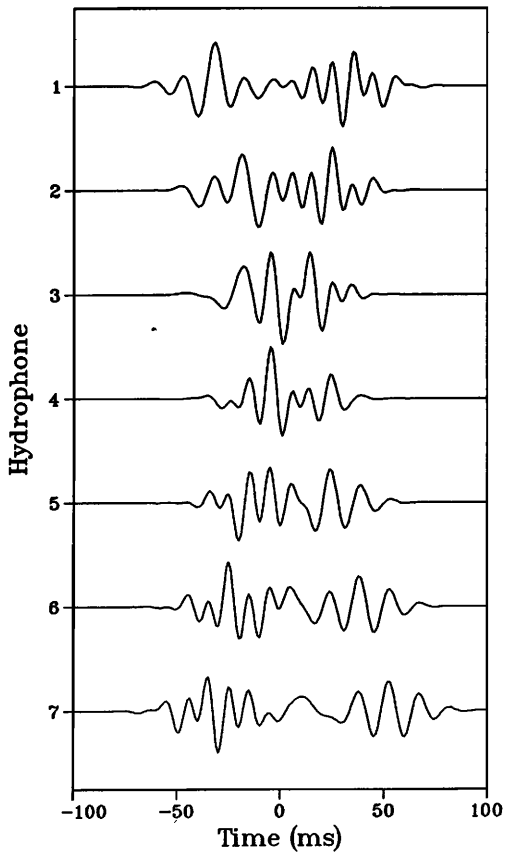


FIG. 2. The received data for example A, which involves the optimal beamformer with seven equally spaced receivers and five sources.

Unless $\theta \cong \theta_m$ for some $m$, the time series in Eq. (8) add incoherently, and

$$B(\theta) = \int [O(N^{1/2})]^2 \, dt = O(N). \tag{9}$$

For $\theta = \theta_m$, the $m$th time series terms add coherently, and

$$B(\theta_m) = \int [Np_m(t) + O(N^{1/2})]^2 dt = O(N^2). \tag{10}$$

Keeping the dominant term in Eq. (10), we obtain

$$B(\theta_m) \sim N^2 \int [p_m(t)]^2 \, dt. \tag{11}$$

For example B, we apply the delay-and-sum beamformer to a problem involving the source bearings and time series of example A. The estimates of $B(\theta_m)$ given by Eq. (11) are approximately proportional to $A_m^2 w_m$ for these sources. We consider four equally spaced arrays: array 1 ($N=7$, $\Delta x=20$ m); array 2 ($N=14$, $\Delta x=20$ m); array 3 ($N=14$, $\Delta x=10$ m); and array 4 ($N=28$, $\Delta x=10$ m). Results for example B appear in Fig. 5. For array 1, which

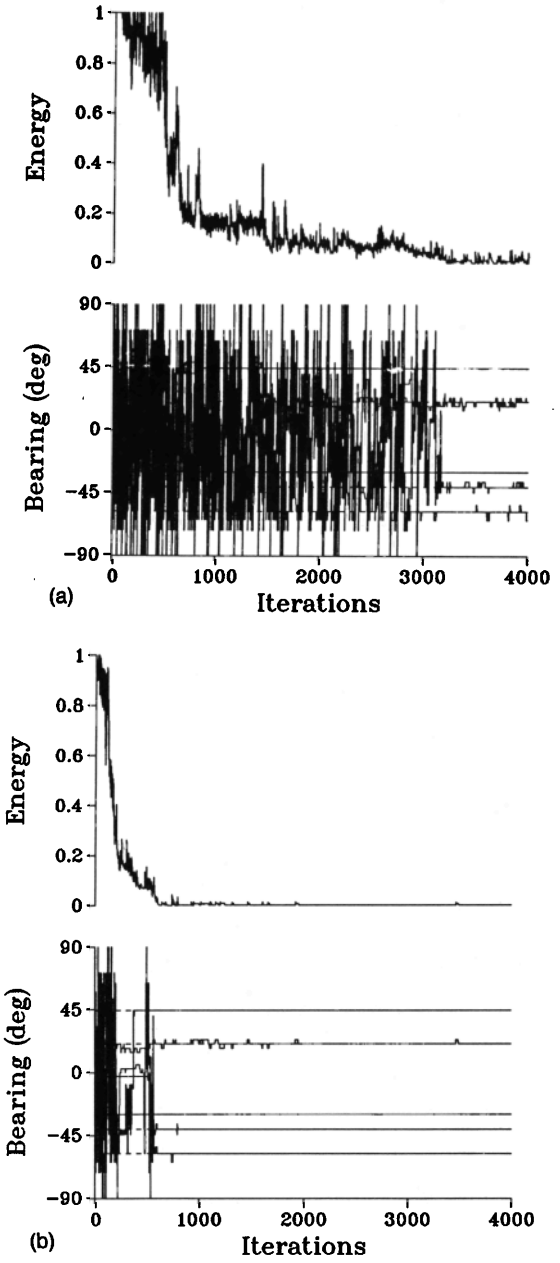


FIG. 3. Results for example A, which involves the optimal beamformer with seven equally spaced receivers and five sources. (a) The original simulated annealing algorithm converges after approximately 3000 iterations. (b) The improved simulated annealing algorithm converges after approximately 500 iterations.

was used successfully with the optimal beamformer in example A, the delay-and-sum beamformer has large false peaks near broadside and endfire. The false peaks are smaller for array 2. Although there are no major false peaks for array 3, two of the weaker source peaks are barely separated from sidelobes. All five of the peaks are well defined for array 4 with levels approximately equal to the values predicted by Eq. (11). Example B illustrates that the optimal beamformer can handle larger receiver spacing and larger source-to-receiver ratio than the delay-and-sum beamformer.

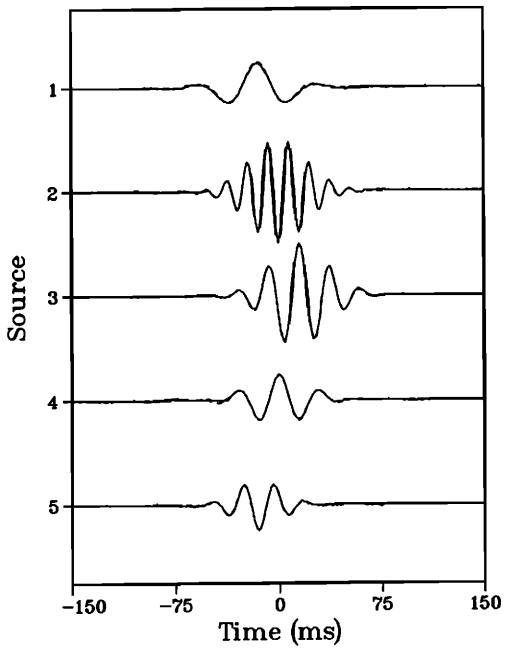


FIG. 4. Results for example A, which involves the optimal beamformer with seven equally spaced receivers and five sources. The time series recovered with the improved algorithm (solid curves) agree with the true time series (dashed curves).

## IV. IRREGULAR RECEIVER SPACING

The performance of a beamforming algorithm is sensitive to the array parameters. For example, the results of Sec. III illustrate the importance of $N$ and $\Delta x$. These are not the only parameters that can be varied. For example, some beamforming methods can be enhanced significantly by selecting the receiver locations so that the array samples a wide range of length scales.[6] In this section, we illustrate the advantage of using irregular receiver spacing with the optimal beamformer.

For example C, we consider the sources of example A and drop the assumption that the source time series have compact support. When the bearings are assumed to be known *a priori*, an evenly spaced array with $N=9$ and $\Delta x=20$ m recovers the source time series appearing in Fig. 6, which are corrupted by the periodic ambiguity. Results appear in Fig. 7 for an array of nine receivers with spacings (from the end of the array corresponding to positive bearing) of 2, 17, 5, 23, 7, 19, 3, and 13 m. We used two more receivers than for example A because some of the receiver spaces are small. With this array, the source bearings are recovered and the recovered time series agree with the true time series with only small hints of the periodic ambiguity.

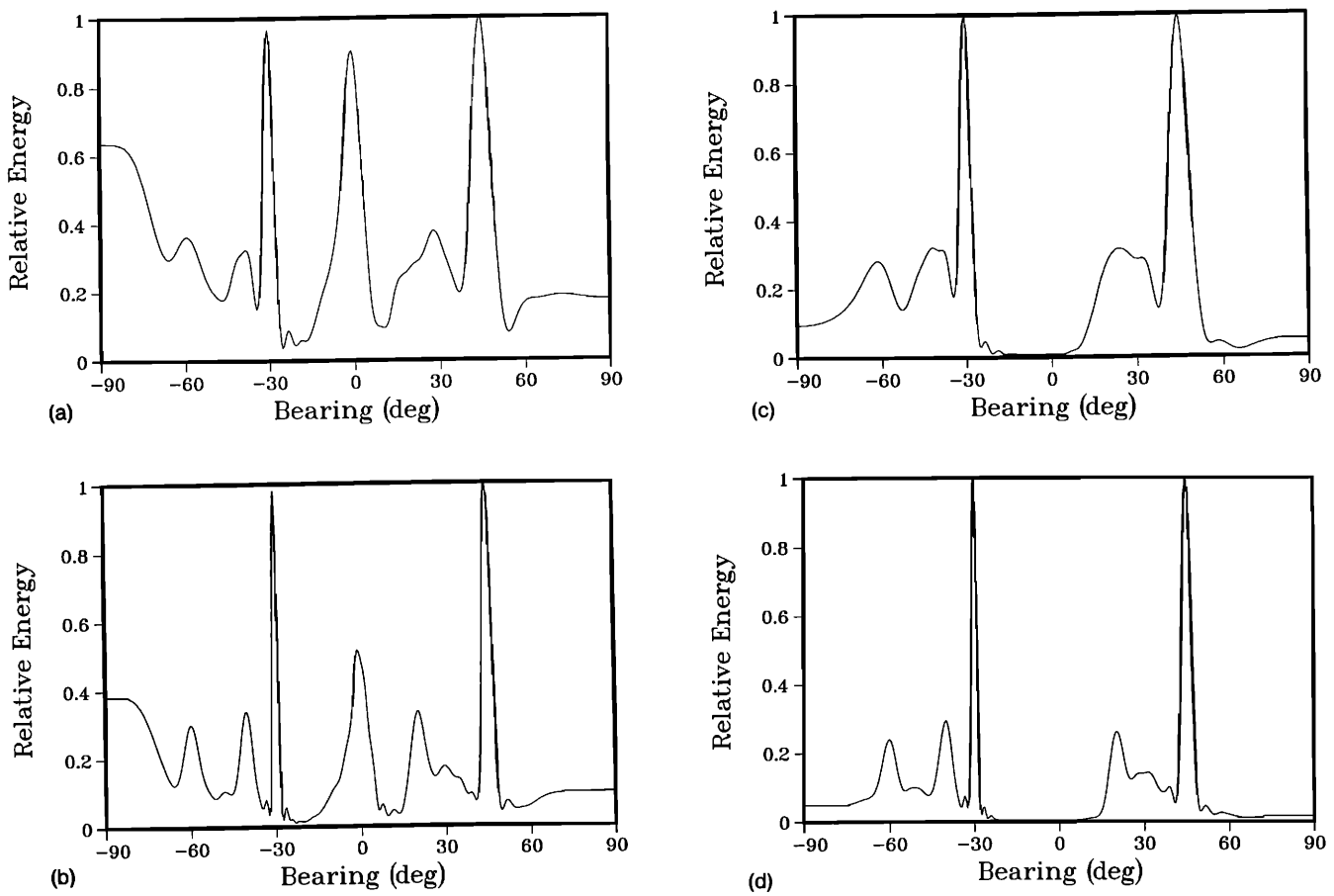


FIG. 5. Results for example B, which involves the conventional delay-and-sum beamformer with equally spaced receivers and five sources. (a) There are large false peaks near broadside and endfire for array 1. (b) The levels of the false peaks are reduced for array 2. (c) Although there are no major false peaks for array 3, two of the source peaks are barely separated from sidelobes. (d) The five source peaks are well defined for array 4.

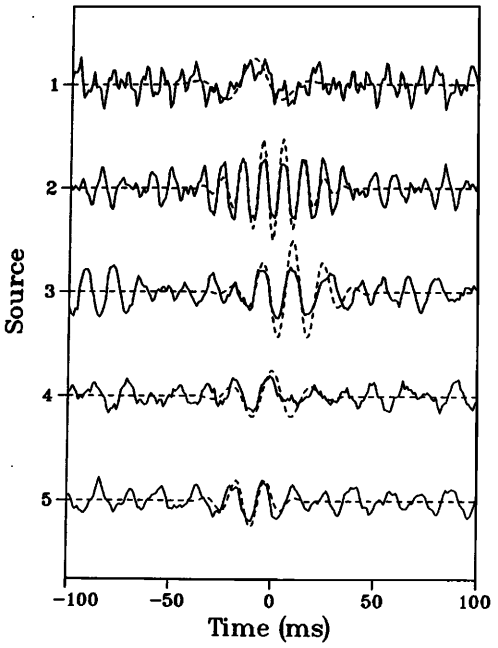


FIG. 6. Results for example C, which involves the five sources of example A without the compact support assumption. Using nine evenly spaced receivers and assuming that the source bearings are known *a priori*, the recovered time series are corrupted by the periodic ambiguity.

## V. FRACTIONAL BEAMFORMING

All beamforming methods have difficulty determining the bearings of weak sources that are dominated by interference from strong sources. In this section, we present an effective approach for handling weak sources with the optimal beamformer. We refer to the approach as fractional beamforming, which involves two steps. The optimal beamformer is first applied to estimate the bearings and time series of the strong sources. If a sufficiently low energy is achieved (this occurs only if the weak sources truly are weak), the strong sources are then subtracted from the data. The optimal beamformer is applied to the reduced data to estimate the bearings and time series of the weak sources. Fractional beamforming often performs much better than the approach of applying the optimal beamformer to search for all of the sources at once. The performance is best when the weak sources are substantially below the strong sources. Similar behavior occurs with an approach for extracting weak signals from noise.[7]

For example D, we consider a problem involving two strong sources, one weak source (20 dB below each of the strong sources), and the irregularly spaced array of example C. The parameter values for the sources are given in Table I. The results of applying the optimal beamformer to estimate the bearings and time series of the strong sources from the raw data appear in Fig. 8. Both of the bearings and time series are recovered accurately modulo a small dc component. The results of applying the optimal beamformer to the reduced data appear in Fig. 9. The bearing of

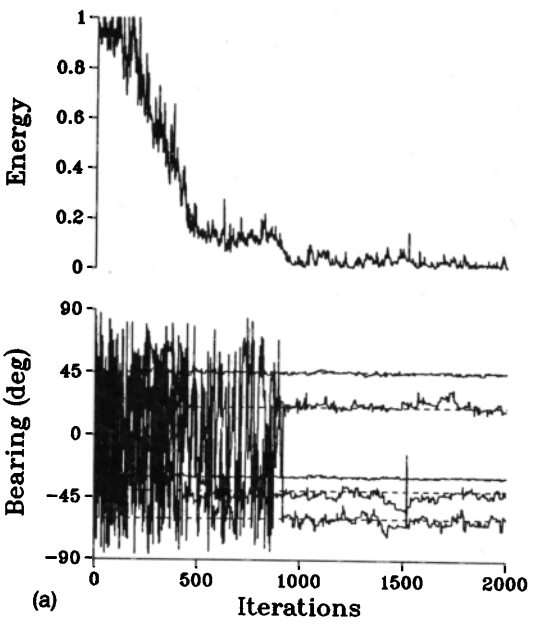


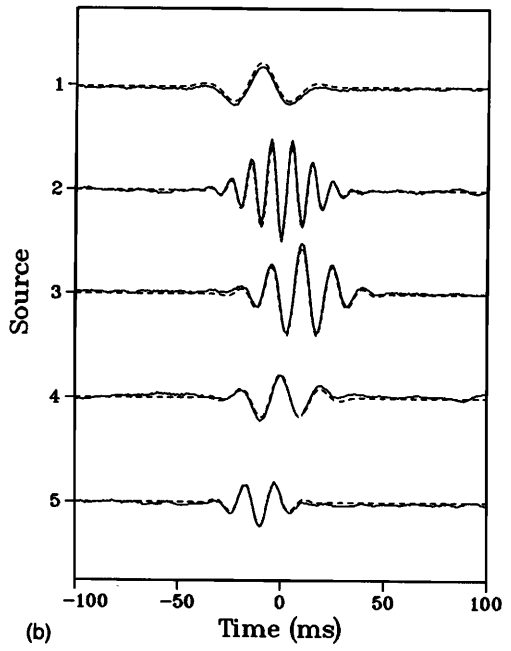


FIG. 7. Results for example C, which involves the five sources of example A without the compact support assumption. Using an irregularly spaced array with nine receivers, the bearings converge to the correct values (a), and the recovered time series (solid curves) and true time series (dashed) curves are in agreement (b).

the weak source is accurately determined. The recovered time series for the weak source is also fairly accurate. The results of applying the optimal beamformer to search for all three sources at once appear in Fig. 10. Although the bearings of the strong sources are recovered, the bearing parameter for the weak source wanders aimlessly.

## VI. NOISE CANCELLATION

The optimal beamformer may be generalized to cancel noise if an appropriate property of the noise is known. In

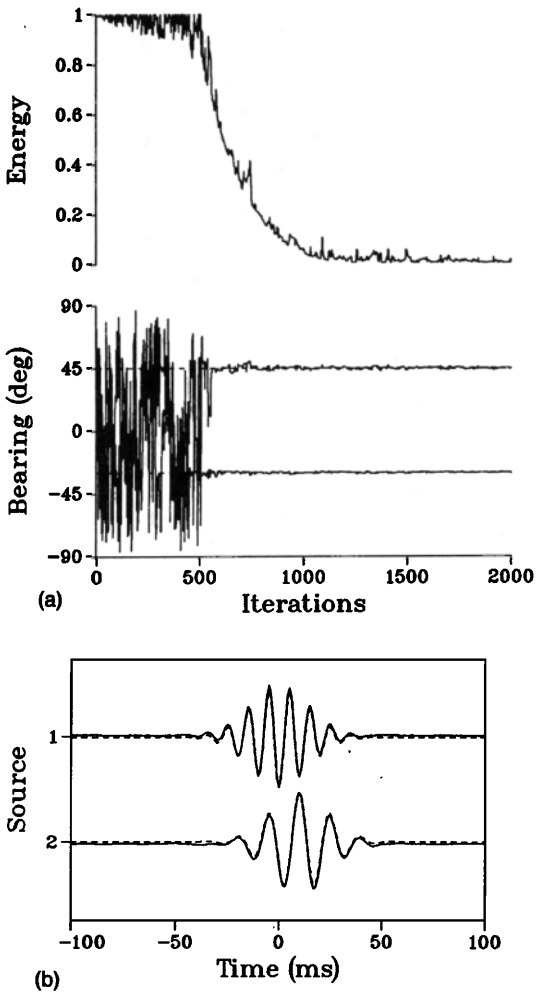


FIG. 8. Results for example D, which involves two strong sources and one weak source. The optimal beamformer is applied to the raw data searching for two sources. For the strong sources, (a) the bearings are recovered, and (b) the recovered time series (solid curves) agree with the true time series (dashed curves) modulo a small dc component of the ambiguity.

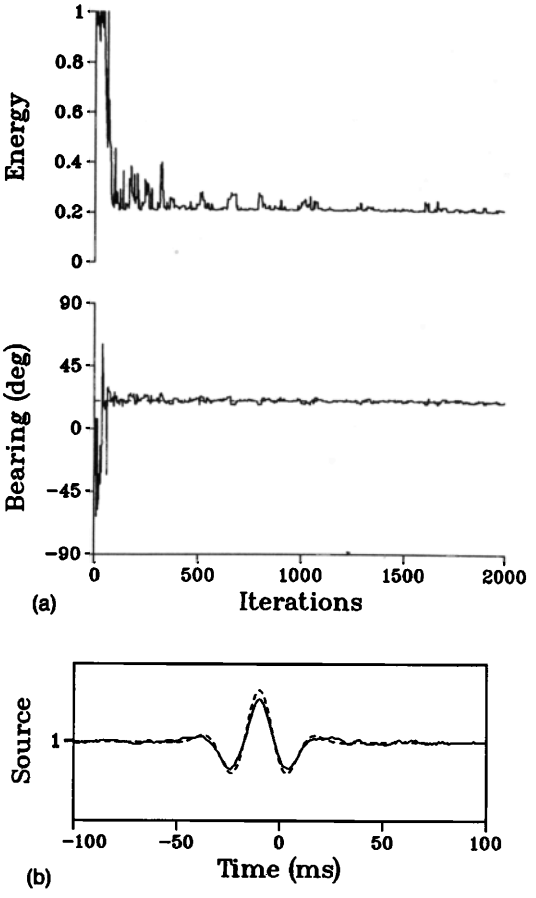


FIG. 9. Results for example D, which involves two strong sources and one weak source. The optimal beamformer is applied to the reduced data searching for one source. For the weak source, (a) the bearing is recovered, and (b) the recovered time series (solid curves) agrees with the true time series (dashed curves).

this section, we modify the optimal beamformer to cancel electromagnetic noise. This type of noise usually consists of discrete frequencies. Although this type of noise can be removed using the Fourier transform, parts of the signals may also be removed with this approach. The cancellation approach, which may be applied to various types of noise, removes noise surgically.

The noise term is assumed to be of the form,

$$\Psi_n(t) = \nu_n \sin(\omega t + \delta), \tag{12}$$

where $\omega$ is the circular frequency of the source. Unless the noise on different receivers arises from different processes, the unknown phase $\delta$ is independent of $n$ (modulo $\pi$) because electromagnetic signals propagate much faster than acoustic signals. The phase may differ by $\pi$ on different receivers (we have observed this in data) if (for example) the noise is generated by a varying magnetic field and

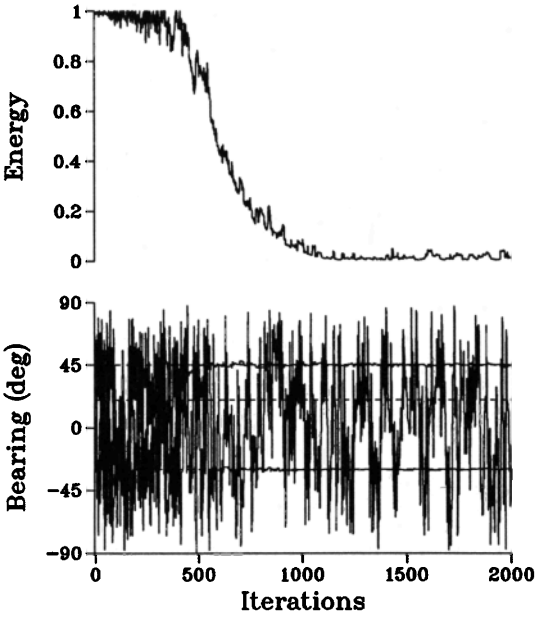


FIG. 10. Results for example D, which involves two strong sources and one weak source. The optimal beamformer is applied to the raw data searching for three sources. The bearings are recovered for the strong sources but not for the weak source.

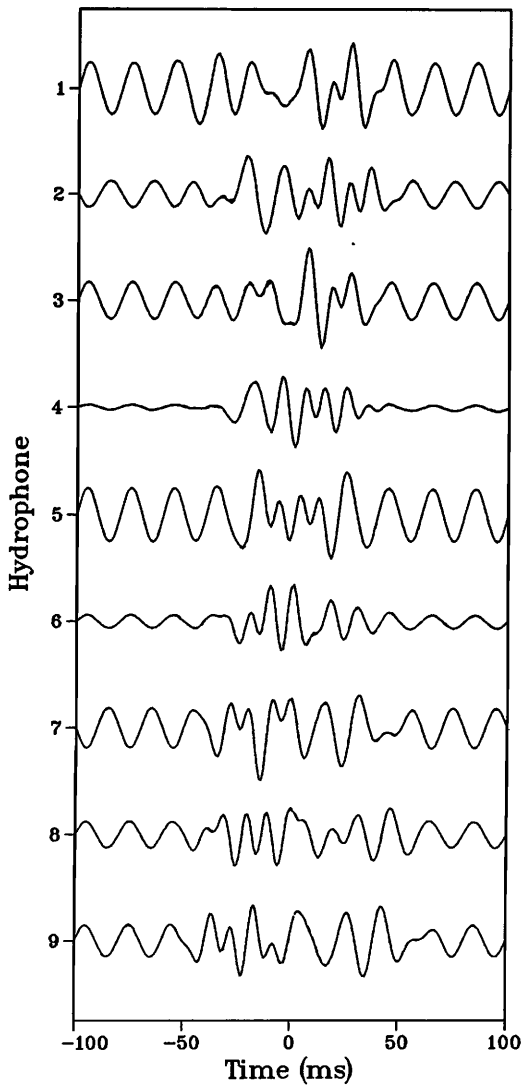


FIG. 11. Data and results for example E, which involves cw noise from electromagnetic interference. The best replica (dashed curve) agrees with the data (solid curve). The highest noise level occurs on receivers 1 and 5.

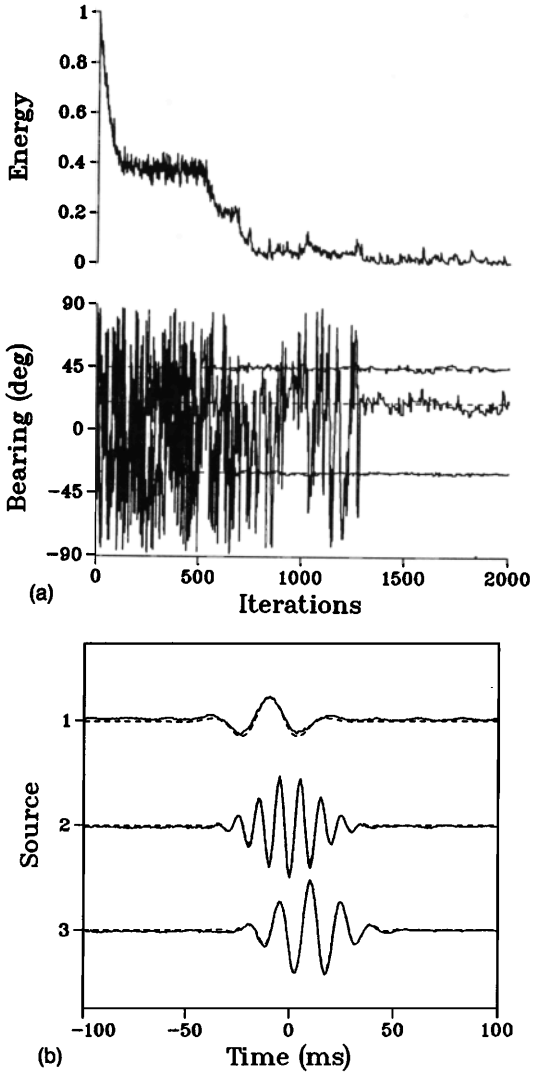


FIG. 12. Results for example E, which involves cw noise from electromagnetic interference. (a) The source bearings are recovered. (b) The source time series are recovered.

the wires corresponding to different receivers are coiled in opposite directions.

The noise amplitudes $\nu_n$ are assumed to depend on $n$ because some receivers may be noisier than others. To account for phase reversals, we allow the sign of $\nu_n$ to depend on $n$. This approach may be applied to cancel noise consisting of several frequencies. The solution is ambiguous if one of the plane waves is incident at broadside. If at least one of the receivers is noise-free, however, this ambiguity may be eliminated by assuming the noise amplitude vanishes for that receiver.

We illustrate noise cancellation with example E, which involves the nine irregularly spaced receivers used in example C and the three sources described in Table I. The 50-Hz noise amplitudes on the receivers are 2.0, −1.0, 1.4, 0.2, 2.0, 0.5, −1.5, 1.0, and 1.2. The noisy array data and the replica time series corresponding to the lowest energy state encountered appear in Fig. 11. Other results for example E appear in Fig. 12. All three of the source bearings

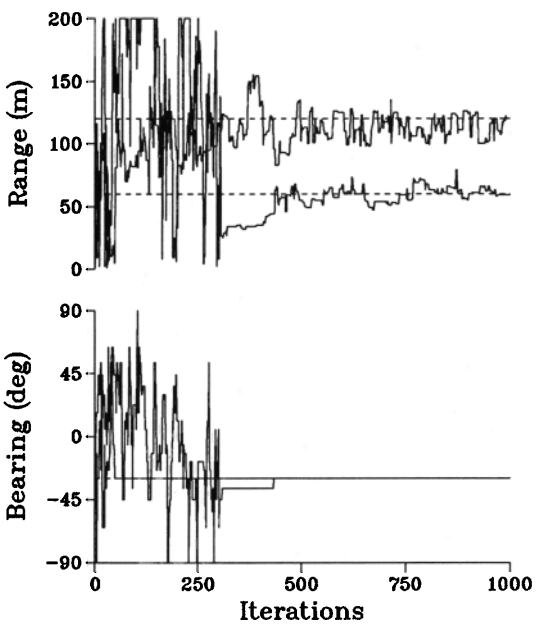


FIG. 13. Results for example F, which involves two-dimensional localization of two point sources located along the same bearing.

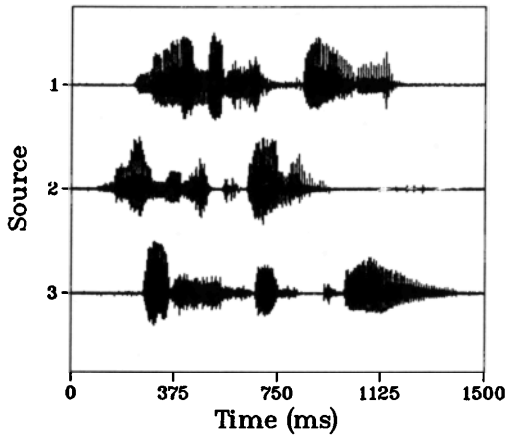


FIG. 14. The phrases for example G, which involves speech processing with three speakers and seven receivers. The phrases (from the top down) are "minus forty," "minus twenty," and "plus fifteen."

are recovered accurately. The source time series and the noise parameters are also recovered.

## VII. SPHERICAL WAVES

In this section, we modify the optimal beamformer to handle incident spherical waves. This approach is applicable when some of the sources are less than about ten array lengths away. For this problem, spherical spreading is included and the delays appearing in Eqs. (1) and (2) are modified to be

$$\tau_n = \frac{|\mathbf{x}-\mathbf{x}_n|}{c}, \tag{13}$$

where $\mathbf{x}$ is the source location and $\mathbf{x}_n$ is the location of the $n$th receiver. The coordinate origin is taken to be the centroid of the array. If the receivers are collinear, it is possible to determine the two source coordinates corresponding to range $r$ and bearing $\theta$.

Example F involves two sources located on the same bearing $\theta = -30$ deg at $r = 60$ m and $r = 120$ m. We use an array of seven equally spaced receivers with $\Delta x = 10$ m and the source parameters appearing in Table I. Results for example F appear in Fig. 13. The algorithm converges quickly, and the bearings are recovered accurately. The range of the closer source is recovered with more certainty

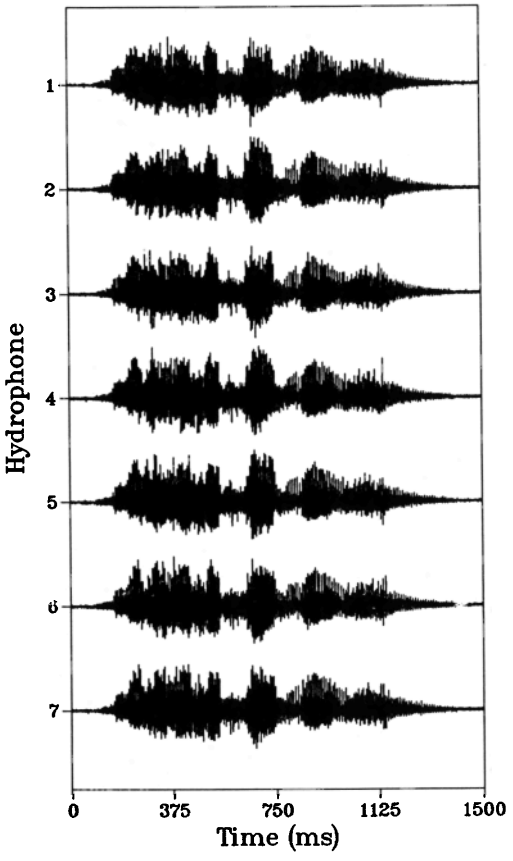


FIG. 15. The array data for example G, which involves speech processing with three speakers and seven receivers.

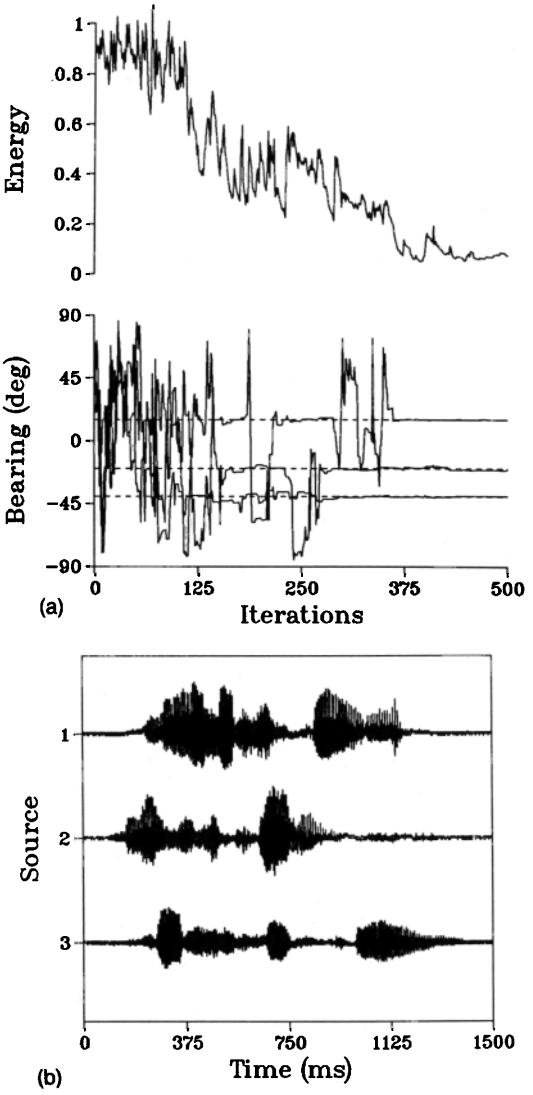


FIG. 16. Results for example G, which involves speech processing with three speakers and seven receivers. (a) The bearings of the speakers, which are the same as the phrases (in degrees), are recovered. (b) The recovered phrases agree with the true phrases appearing in Fig. 14.

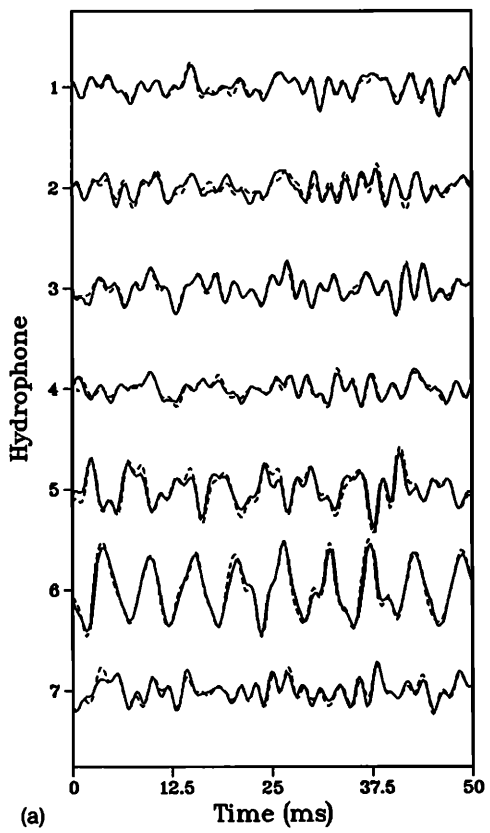


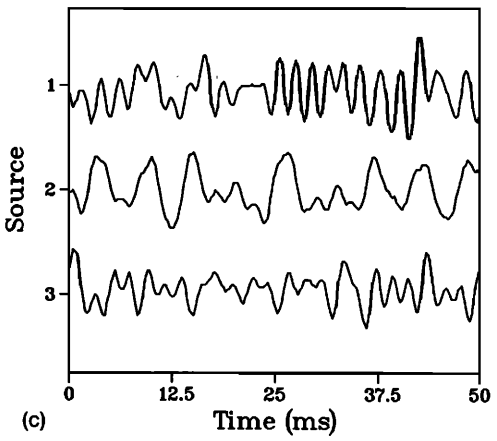


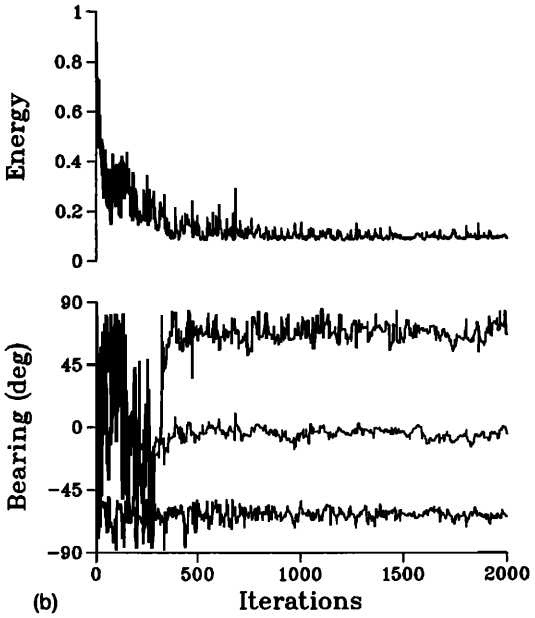


FIG. 17. Results for the first data segment of example H, which involves data from the Atlantic Ocean. (a) The array data (dashed curve) and the best replica (solid curve). Note the 180-Hz noise on receivers 5 and 6. (b) The energy and the source bearings. (c) The recovered time series for the tow ship (source 1), the passing ship (source 2), and the distant ship (source 3).

because its wave-front curvature is easier to resolve with this array. The source range becomes a weak attractor (i.e., the parameter does not tend to remain near the true value during the search) as it increases. This beamformer reduces to the plane-wave optimal beamformer in the limit of large source range.

## VIII. SPEECH PROCESSING

In this section, we apply the optimal beamformer to example G, which is a speech-processing problem involving complex signals and more than 70 000 unknowns. The phrases "minus forty," "minus twenty," and "plus fifteen" were digitized using a NeXT computer. These phrases, which appear in Fig. 14, were each recorded separately for 1.5 s using a 16-kHz sampling rate. The phrases were then superimposed using Eq. (1) to simulate data on an evenly spaced array with $N=7$ and $\Delta x=0.5$ m. The array data appear in Fig. 15. These jumbled phrases sound similar from receiver to receiver. The bearings used for the speakers (in degrees) correspond to the phrases. We assumed that $c=300$ m/s.

Although the array data are quasisynthetic, this problem differs from the simulations presented in previous sections in that the signals are highly complex and the number of parameters is much larger. The results of the simulated annealing algorithm appear in Fig. 16. The bearings of the speakers are recovered accurately, and the recovered phrases, which sound nearly identical to the original phrases, are similar to the true phrases. Phrase 1, which contains more energy than the other phrases, is recovered with the greatest accuracy.

Due to the large number of time series points, it took several hours to solve this problem on a SiliconGraphics Iris workstation. Since the optimal beamformer is parallel in the time series parameters, however, run time on a parallel processing computer would be essentially independent of the number of time series points.

## IX. OCEAN ACOUSTIC DATA

In this section, we apply the optimal beamformer to data from a 64-receiver array towed behind the USNS LYNCH in a region of the Atlantic Ocean south of Nova Scotia. The array consists of four nested subarrays with even spacings of 1.25, 2.5, 5, and 10 m. The system was not designed for the optimal beamformer. The receiver spacings were not optimized to suppress the periodic ambiguity. Some receivers exhibited a large amount of 180-Hz electromagnetic noise, which is not a problem for the frequency-domain processors for which the array was designed. We took 2-s data segments every half-hour using a 2-kHz sampling rate and an analog filter to remove energy above 500 Hz. We were able to obtain solutions with the optimal beamformer and verify them in nearly real time using radar and conventional frequency-domain processing with larger subarrays. We assumed that $c=1500$ m/s for the data presented here, which was taken on 14 August 1990 near 42.7 deg N, 62 deg W. The ocean is approximately 1400 m deep in this area. The LYNCH towed the array toward the southeast at 3 kn.

For example H, we consider portions of three consecutive data segments (a total time of about 1 h) that contain signals from the tow ship, a passing ship that was sweeping in bearing, and a distant ship that remained near aft endfire. We worked with an evenly spaced subarray of seven receivers with $\Delta x=2.5$ m. Since the 180-Hz noise was observed to be weak on receivers 1, 2, and 3, we assumed that the noise vanishes on these receivers to suppress the broadside ambiguity described in Sec. VI. We searched for three sources applying the *a priori* knowledge that the tow ship was near endfire. Since the array was submerged, we allowed the tow ship to be up to 40 deg from endfire. We searched for only two sources in the third data segment because the passing ship and the distant ship were both near endfire.

Results for the first data segment appear in Fig. 17. The array data and the best replica (i.e., the replica corresponding to the lowest energy encountered) are in good agreement. The 180-Hz noise levels on receivers 5 and 6 are relatively high. The recovered source bearings correspond to the true bearings of the passing ship and the distant ship. The bearing recovered for the tow ship indicates that the array dipped to about 25 deg below endfire. The recovered signal for the passing ship contains lower frequencies than the other signals. All of the receivers appear to be free of 180-Hz noise in the reduced data, which consists of the data minus the best 180-Hz noise replica and appears in Fig. 18. Results for the second and third data segments appear in Figs. 19 and 20. The data and replica time series are in good agreement for both of these cases. For the second segment, the passing ship is louder than the other ships. For the third segment, the combined signal from the passing ship and the distant ship is weaker than the tow ship signal.

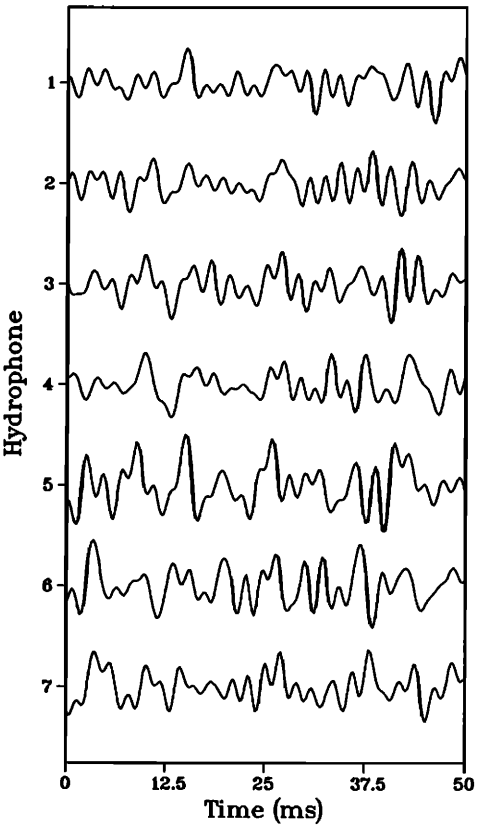


FIG. 18. Reduced array data for the first data segment of example H, which involves data from the Atlantic Ocean. The 180-Hz noise on receivers 5 and 6 has been canceled.

To illustrate the ability of the optimal beamformer to surgically remove signals from data, we consider example I, which involves the second segment of data and an evenly spaced subarray of nine receivers with $\Delta x=5$ m. These array parameters were selected so that conventional beamforming would perform well for lower frequencies. A frequency-azimuth (FRAZ) diagram (which displays beamformed energy versus frequency and azimuth) of the raw data appears in Fig. 21(a). To construct this diagram, 0.5 s of data was used to estimate the spectrum, and the Bartlett processor was evaluated for 181 bearings and 220

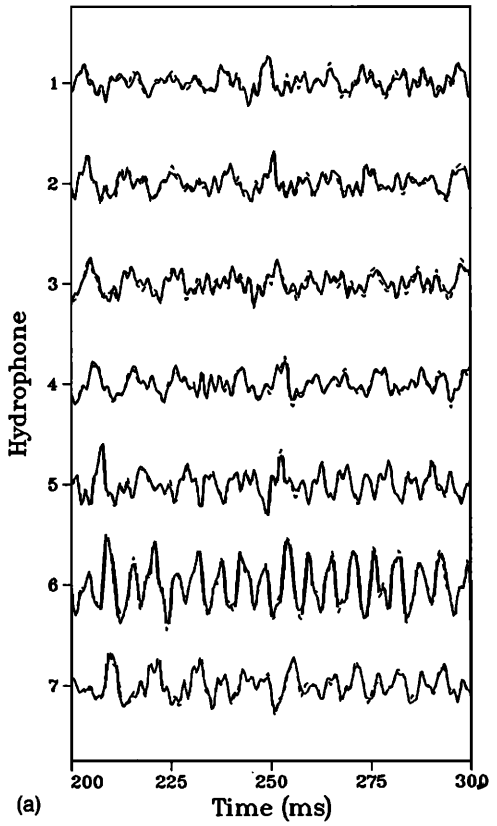


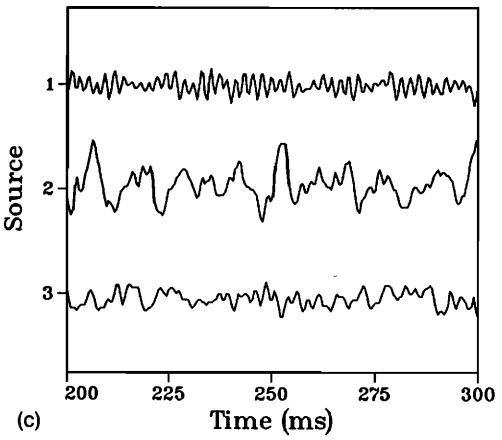


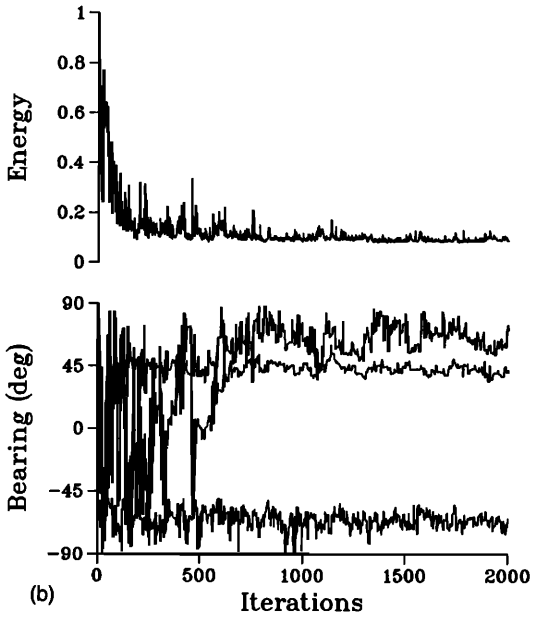


FIG. 19. Results for the second data segment of example H, which involves data from the Atlantic Ocean. (a) The array data (dashed curve) and the best replica (solid curve). (b) The energy and the source bearings. (c) The recovered time series for the tow ship (source 1), the passing ship (source 2), and the distant ship (source 3).

frequencies. The passing ship appears near $\theta=40$ deg and the other ships appear near the opposite endfire positions. There are numerous sidelobes for the three sources. These false peaks can be distinguished from true source peaks because their locations vary with frequency. Although the electromagnetic noise is evident at various multiples of 60 Hz (especially 180 Hz), it is weak relative to the broadband acoustic signals, and we do not bother to cancel it in this subarray.

Using the *a priori* information gained from example H, we initialized the temperature at a low value and restricted the source bearings to narrow windows. After 200 iterations, the algorithm produced results similar to the results of example H. A FRAZ diagram appears in Fig. 21(b) for the reduced data obtained by subtracting the best tow-ship replica from the data. All evidence of the tow ship is gone including its sidelobes. The features corresponding to the other ships do not appear to be affected. Appearing in Fig. 21(c) is the FRAZ diagram of the data minus the best replicas for the tow ship and the passing ship. The peaks corresponding to the distant ship and its sidelobes remain intact. The FRAZ diagram obtained by subtracting all

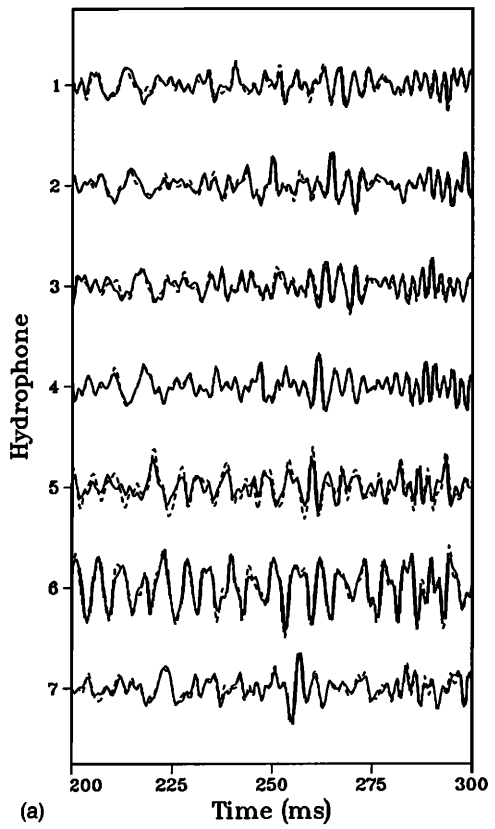


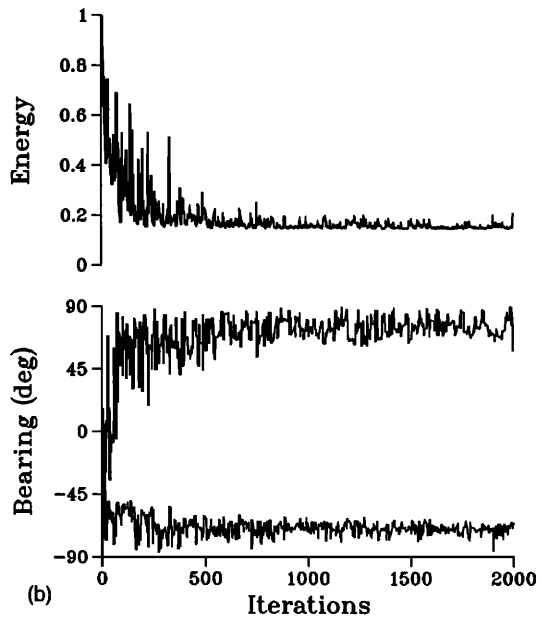


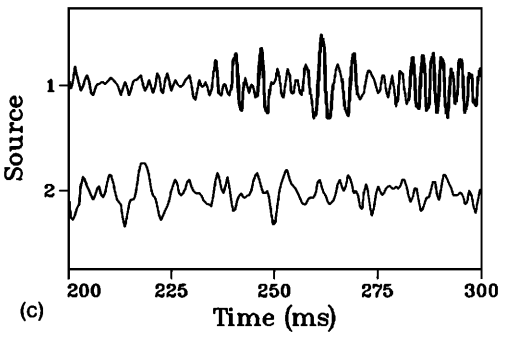


FIG. 20. Results for the third data segment of example H, which involves data from the Atlantic Ocean. (a) The array data (dashed curve) and the best replica (solid curve). (b) The energy and the source bearings. (c) The recovered time series for the tow ship (source 1) and the passing ship and distant ship combined (source 2).

three best replicas appears in Fig. 21(d). Evidence of a fourth signal near $\theta=20$ deg appears in the low-frequency region of the diagram.

## X. CONCLUSION

An improved simulated annealing algorithm has been developed for the optimal beamformer. By accepting time series perturbations only if the energy function decreases, convergence is accelerated and high-frequency noise associated with the periodic ambiguity is suppressed. Fractional beamforming is an effective approach for handling weak sources. The optimal beamformer handles larger receiver spacings and more sources per receiver than conventional beamformers, which collapse all of the unknowns into a single parameter. By using irregular receiver spacing, the performance of the optimal beamformer may be enhanced and the low-frequency component of the periodic ambiguity may be suppressed. It is possible to cancel certain types of noise with the optimal beamformer if the nature of the noise is understood. The optimal beamformer performs well for towed array data and for speech processing.

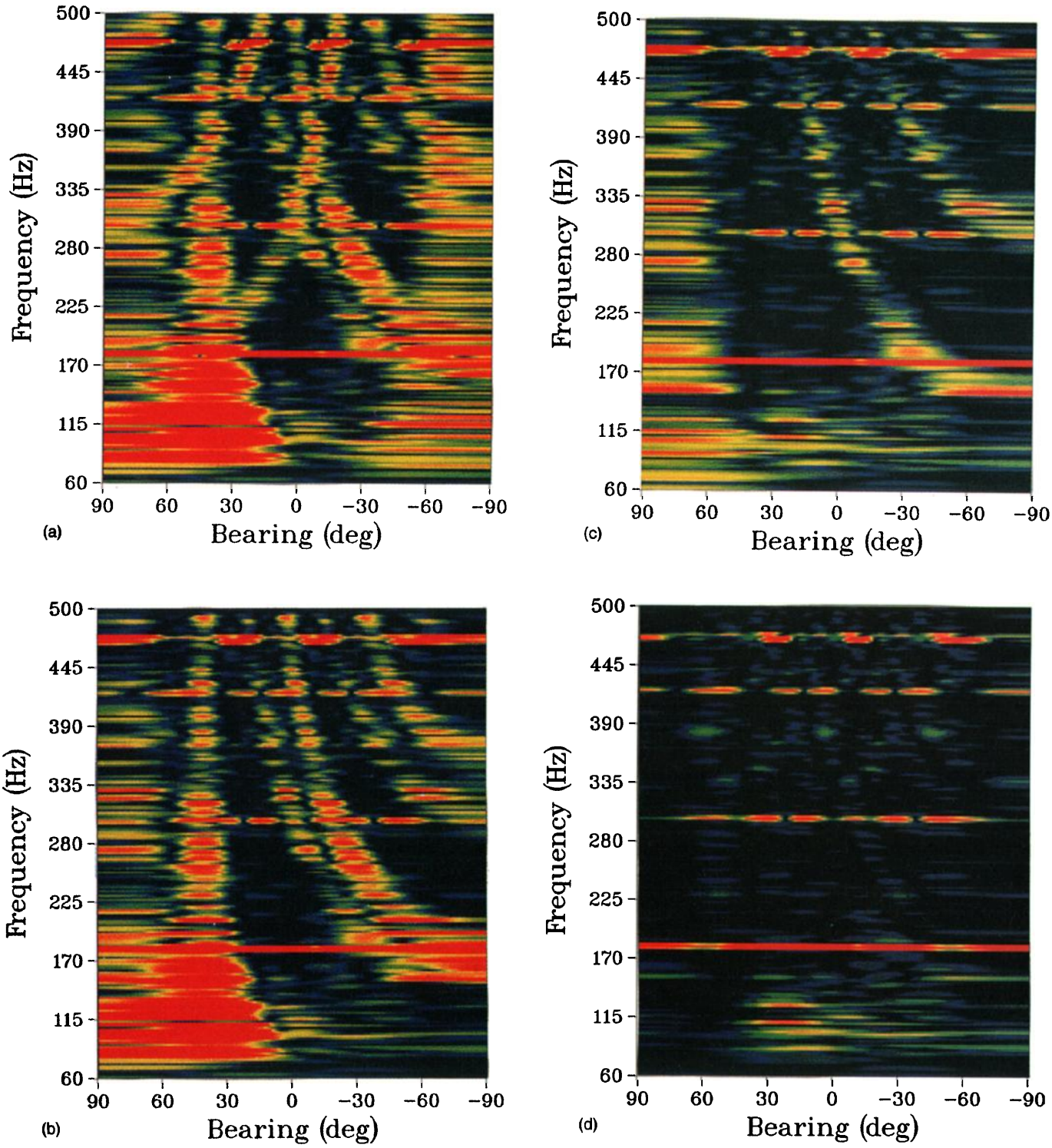


FIG. 21. Results for example I, which involves data from the Atlantic Ocean. FRAZ diagrams for (a) the raw data; (b) the raw data minus the best tow ship replica; (c) the raw data minus the best tow ship and passing ship replicas; and (d) the raw data minus all three replicas. The colors span 20 dB, with red corresponding to high intensity and blue corresponding to low intensity.

## ACKNOWLEDGMENTS

The authors thank G. Gibian and R. Pitre for digitizing the phrases for the speech-processing example and N. Davis, T. Krout, and B. Pasewark for participating in the experiment on the USNS LYNCH.

[1] W. A. Kuperman, M. D. Collins, J. S. Perkins, and N. R. Davis, "Optimal time-domain beamforming with simulated annealing including application of *a priori* information," J. Acoust. Soc. Am. **88**, 1802–1810 (1990).

[2] K. C. Sharman, "Maximum likelihood parameter estimation by simulated annealing," in *Proceedings of the IEEE Conference on Acoustics,*

*Speech, and Signal Processing*, pp. 2741–2744 (1988).
[3]N. Metropolis, A. W. Rosenbluth, M. N. Rosenbluth, A. H. Teller, and E. Teller, "Equations of state calculations by fast computing machines," J. Chem. Phys. **21**, 1087–1091 (1953).
[4]S. Kirkpatrick, C. D. Gellatt, and M. P. Vecchi, "Optimization by simulated annealing," Science **220** (4598), 671–680 (1983).
[5]H. Szu and R. Hartley, "Fast simulated annealing," Phys. Lett. **122**, 157–162 (1987).
[6]S. W. Lang, G. L. Duckworth, and J. H. McClellan, "Array design for MEM and MLM array processing," *Proceedings of the IEEE Conference on Acoustics, Speech, and Signal Processing*, pp. 145–148 (1981).
[7]G. J. Orris, B. E. McDonald, and A. Kuperman, "Phase-matching filter techniques for low signal-to-noise data," J. Acoust. Soc. Am. **91**, 2444 (1992).